Puckered in pioneer neurons coordinates the motor activity of the *Drosophila* embryo

Katerina Karkali[1,3], Samuel W. Vernon[2], Richard A. Baines[2], George Panayotou[3] and Enrique Martín-Blanco[1] *

1. Instituto de Biología Molecular de Barcelona (CSIC), Parc Cientific de Barcelona, Baldiri Reixac 10-12, 08028 Barcelona, Spain

2. Division of Neuroscience and Experimental Psychology, School of Biological Sciences, Faculty of Biology, Medicine and Health, University of Manchester, Manchester Academic Health Science Centre, Manchester, M13 9PL, UK.

3. BSRC Alexander Fleming, 34 Fleming Street, 16672 Vari, Greece

* Correspondence to: embbmc@ibmb.csic.es

SUMMARY

Central Nervous System (CNS) organogenesis is a complex process that obeys precise architectural rules. The impact that nervous system architecture may have on its functionality remains, however, relatively unexplored. To clarify this problem, we analyzed the development of the Drosophila embryonic Ventral Nerve Cord (VNC). VNC morphogenesis requires the tight control of Jun kinase (JNK) signaling, exerted in part via a negative feedback loop mediated by the dual specificity phosphatase Puckered, in a subset of pioneer neurons. Here we show that the JNK pathway autonomously regulates neuronal electrophysiological properties without affecting synaptic vesicle transport. Manipulating, during early embryogenesis, JNK signaling activity in pioneer neurons, directly influences their function as 'organizers' of VNC architecture and, moreover, uncovers a role in the coordination of the embryonic motor circuitry that is required for hatching. Together, our data reveal critical links, mediated by the control of the JNK signaling cascade by Puckered, between the structural organization of the VNC and its functional optimization.

INTRODUCTION

Nervous system architecture is the outcome of neuro-glial interactions and axon guidance decisions. Yet, how the nervous system achieves a mechanically balanced organization while functional neuronal connectivity is established throughout morphogenesis is poorly understood. Several lines of evidence suggest a direct relationship between the 3D architectural organization of the nervous system and its functionality. First, the spatial distribution of functional circuits in the cortex of vertebrates extensively overlaps with large-scale microstructure, connectivity, and gene expression patterns [1]. Second, in pursuit of functional efficiency, neural networks likely minimize their structural cost following the wiring optimization principle postulated by Ramón y Cajal [2]. These costs likely arise from metabolic requirements, signal delay and attenuation, and complex guidance processes [3] that increase with interneuronal distance [4]. Lastly, the spatial organization of cortical areas appears subjected to evolutionary selection [5].

We have recently shown that the acquisition of the *Drosophila* embryonic Ventral Nerve Cord (VNC) specific 3D neural architecture is directed by the mechanical coordination of neurons and glia [6]. Further, we have also uncovered that a precise modulation of the activity of the JNK signaling cascade, in a subset of early specified neurons, is required for proper VNC architectural organization and its condensation (Karkali et al, co-submitted). We now determine whether accuracy in nervous system spatial organization/topography is essential for functionality. In particular, by employing the VNC as a model system, we asked if JNK-mediated modulation of VNC architecture is essential for the emergence of the coordinated embryonic motor circuit activity that mediates larval hatching [7]

The best-known role of the JNK signaling cascade in the nervous system is to coordinate the induction of protective genes in response to oxidative (ROS) challenges [8] and axonal regeneration [9]. Yet, JNK has been found to mediate multiple functions in the CNS both in *Drosophila* and mice, including axonal growth [10]; axonal organelle (mitochondrial) and synaptic protein transport [8, 11, 12, 13, 14]; synaptic growth and synaptic strength [15]; dendrite pruning [16]; self-renewal of neuronal precursors [17]; neuronal migration [18]; glia remodeling [19] and neuronal neuroplasticity (reviewed in [20]). Further, and importantly, it is well established that some of the effects of JNK activation in the CNS do not proceed through the regulation of the transcription machinery (AP1), and likely occur via phosphorylating cytoplasmic targets in the soma [8, 13]. In this scenario, we hypothesize that the JNK pathway may have a regulatory role in the optimization of neural function, associated with the structural organization of the VNC.

63 During VNC condensation, *Drosophila* embryos develop sporadic muscle contractions that
64 initially do not correlate with sensory input [21, 22]. Yet, over time, these contractions evolve into
65 coordinated peristaltic patterns, dependent on a precise coordination of the contractile activity
66 of the embryonic muscles, bilaterally and along the antero-posterior (AP) axis [7]. Here, we
67 uncover essential functions for the JNK pathway in a subset of pioneer neurons enabling the
68 emergence of coordinated motor activity. Early in embryogenesis, a tight control of JNK
69 signaling is necessary, to attain an accurate axonal scaffold organization and native dendrites
70 and axons conformation. Moreover, it is essential for the development of the complex pattern
71 of muscle activities leading to hatching behavior. At later embryonic stages, JNK activity
72 seemingly fine-tunes cell soma location and dendritic morphology and number. Likewise,
73 axonal transport of synaptic vesicles appears to be unaffected by JNK activity, but is critical,
74 upon synaptic input in pioneer motoneurons, for reaching the right Resting Membrane Potential
75 (RMP) to support action potential firing. Combined, our data uncover fundamental structural
76 and physiological roles for the JNK signaling pathway in pioneer neurons linked to embryonic
77 motor pattern optimization.

78

79 **RESULTS**

80 **The level of JNK activity in pioneer neurons is essential for embryonic motor**
81 **coordination**

82 Considering the roles of JNK signaling on promoting VNC architectural robustness (Karkali et
83 al, co-submitted), we investigated the potential functional consequences of releasing the
84 negative feedback control of JNK activity implemented by Puc. We first focused on motor
85 circuits and evaluated late embryonic activity patterns [7, 21] (**Figure 1A** and **1B**) (see **Methods**
86 and **Movie S1**). In wild type conditions, developing embryos execute forward and backward
87 waves of peristalsis by coordinating bilaterally symmetrical muscle contractions [7, 23]. We found
88 that these movements matured through five stages (**Figure 1C**): they began with brief, isolated,
89 unilateral twitches and sporadic head pinching (stage A). This initial phase was followed by a
90 prolonged rest period, occasionally interrupted by uncoordinated single contractions, (B) and
91 then by an active stage showing frequent incomplete and complete peristalsis (C). The active
92 peristalsis stage precedes a short resting period (D), prior to the violent head movements and
93 multiple complete peristaltic events (E) leading to the rupture of the vitelline membrane and
94 larval hatching (see also **Figure S1** and **Movie S2**). In the complete absence of *puc* (*puc*^{E69}),

95 when embryos fail to condense their VNC (Karkali et al, co-submitted), the progression of
96 motor patterns was interrupted, and embryos remained indefinitely in an immature stage (A)
97 characterized by occasional unilateral twitches and incomplete peristalsis (**Figure 1D** and
98 **Movie S3**). Muscle integrity and functionality were not affected.

99 The systemic failure of motor coordination observed in *puc* mutants could be a direct
100 consequence of the increase of JNK activity levels in the CNS or the outcome of other non-
101 defined non-autonomous events. To discard this last possibility, we mimicked *puc* loss of
102 function in different subsets of *puc* expressing neurons such as the aCC, pCC and RP2 pioneers
103 (RN2 Gal4) and the VUM midline neurons (MzVUM Gal4) by overexpressing a constitutively
104 active form of the JNKK ($Hep^{CA)}$). Importantly, interfering in JNK activity in these cells results
105 in architectural defects and in VNC condensation arrest (Karkali et al, co-submitted). For RN2
106 (**Figure 2B** and **2C**) or MzVum cells (**Figure 2D** and **2E**), an excess of JNK activity resulted
107 in a phenotype equivalent to that observed in puc^{E69} mutant embryos. Only occasional unilateral
108 twitches, head pinches and infrequent incomplete peristalsis were observed. Consequently, the
109 motor defects observed in *puc* appear to be a direct response to the loss of Puc activity in
110 specific *puc*+ neurons. The misregulation of the JNK activity links both VNC structural and
111 embryonic motor coordination defects.

112

113 **JNK signaling does not influence synaptic vesicle transport but modulates motoneuron**
114 **firing**

115 Would the loss of embryo motor synchrony after altering JNK activity in *puc*-expressing
116 neurons be consequence of the aberrant architectural organization and inability of the VNC to
117 condense? Some *puc*+ cells are motoneurons and at anomalous levels of JNK activity, their
118 signaling capability might be impaired. This might result in defects in the embryo's motor
119 coordination independently of the VNC architectural organization. To evaluate this possibility,
120 we first studied the axonal transport of synaptic vesicles (Synaptotagmin - Syt) and organelles
121 (Mitochondria - Mito) in the intersegmental nerve [aCC and RP2 (RN2-Gal4) and in VUM
122 motoneurons (MzVum-Gal4)] (see **Methods**, **Figures 3 and S2** and **Movie S4**). Both in RN2
123 and MzVum axons, synaptotagmin particles moved at a speed of around 0,7 µm/s with a
124 tracking lifetime of 50 s per event. Mitochondria run at the same average speed but these
125 movements were less persistent and remained on track 30 s on average. Particles densities
126 (frequency of events) were equivalent for synaptotagmin and mitochondria but larger for aCC

127 and RP2 (0,3 N/µm) than for VUMs (0,2 N/µm). No differences were observed between
128 anterograde and retrograde transport. Next, we analyzed particle transport upon co-expression
129 of Hep^{CA}. Synaptotagmin vesicles kinematic behavior was largely unaffected (**Figure S2**),
130 which indicates that microtubule-mediated transport remained fully functional. The density of
131 traveling mitochondria, however, dropped in aCC and RP2 and increased in VUMs (**Figure 3**),
132 yet sustaining their average lifetime. We noticed the presence of a subpopulation of fast moving
133 mitochondria that could reach a speed of up to 3 µm/s. As for the wild type, we could not
134 distinguish differences between anterograde and retrograde transport. In conclusion, transport
135 of vesicles to synaptic terminals does not seem to be affected by the deregulation of JNK
136 activity. Mitochondrial mobility, however, possibly as a result of altered energetic demands,
137 became anomalous.

138 To directly address if the JNK activity influences motoneuron function, we undertook patch
139 clamp recordings from the aCC and RP2 motoneurons, which receive identical cholinergic
140 synaptic inputs [24]. Neurons were voltage-clamped at -60mV to record endogenously produced
141 cholinergic synaptic currents [Spontaneously Rhythmic Currents (SRCs)]. We found that
142 expression of Hep^{CA} in RN2 + neurons did not influence SRC amplitude or frequency (**Figure**
143 **4A** and **4B**), indicating that the synaptic input to aCC/RP2 remained unaffected. However,
144 current clamp recordings, in which no holding potential was applied (I=0), revealed that the
145 motoneuron Resting Membrane Potential (RMP) was significantly increased and the
146 membrane hyperpolarized (**Figure 4C** and **4D**). Therefore, the average number of action
147 potentials fired per Excitatory Post Synaptic Potential (EPSP) was also notably reduced. We
148 conclude that although the synaptic drive was normal, upon JNK hyperactivation, due to a more
149 negative RMP, excitability, and thus endogenous firing, was considerably reduced in pioneer
150 motoneurons.

151

152 **JNK signaling influences the axodendritic organization of *puc*-expressing neurons**

153 The JNK signaling pathway does not affect synaptic vesicle transport or neuron sensory
154 competencies but modulates their firing response. Could this be related to potential alterations
155 on pioneer neuron morphology and dendrite integrity? To explore this possibility, we
156 examined, for structural defects, the morphology of *puc*-expressing pioneer neurons [RN2
157 (aCC, pCC and RP2)] upon Hep^{CA} overexpression.

158 aCC is a motoneuron whose axon gets incorporated into the intersegmental nerve (ISN) [25]. Its

159 dendritic arbor develops in a distinct region of the ISN myotopic dendritic domain and consists
160 of 8 to 10 dendrites [26] of an average length of 4 µm. pCC is a medially-located interneuron
161 whose axon extends ipsilateral, in an anterior direction [27]. Finally, RP2 is a motoneuron, whose
162 axon proceeds through the posterior root of the ISN [25, 28] and branches out between 7 and 9
163 dendrites, with an average length of 4 µm (**Figure 5A**).

164 As a consequence of the overexpression of Hep^{CA} in RN2+ neurons, the cell bodies of the aCC,
165 pCC and RP2 were frequently misplaced and came together towards the midline (compare
166 **Figures 5A** and **5B**). The appearance of their axons was also affected; they thickened (**Figure**
167 **5B**), increased in length (for pCC and RP2) (**Figure 5C**) and developed a distinctly different
168 wiggly morphology (**Figure 5D**). JNK hyperactivation also affected the density (**Figure 5E**)
169 and length (**Figure 5F** and **Movie S5**) of dendrites. Summarizing, increasing JNK activity in
170 specific pioneer neurons leads to local structural and topographical disarrays that could seed
171 for mistaken 3D arrangements and cumulative misrouting, and be related to their impaired
172 functionality.

173

174 **Different temporal roles for the JNK pathway**

175 To define if the inputs of the JNK pathway modulating the structural organization and
176 functional optimization of the VNC are causally related or independent, we evaluated the
177 effects of interfering in the JNK activity levels within the VNC at different times.

178 Programmed temperature shifts between 29 and 18ºC or *vice versa* (see **Methods**) allowed us
179 to selectively overexpress Hep^{CA} early vs late during embryogenesis. The early-only (stage 10-
180 13) hyperactivation of JNK in RN2+ neurons, before the initiation of neural activity [29], was
181 associated with defects on the morphology of dendrites and axons, with axonal scaffold
182 anomalies and with the collapse of RN2+ neurons towards the midline (compare **Figures 6A,**
183 **B and C**). VNC condensation was also affected (**Figure 6E**). Furthermore, although these
184 embryos occasionally hatched, they displayed strong muscle coordination defects with an
185 almost complete absence of bilateral peristalsis (**Figure 6F** and **Movie S6**). Conversely, the
186 late hyperactivation of the JNK pathway (stage 15-16) did not affect VNC condensation,
187 neither motor coordination and peristalsis (**Figures 6E** and **6F** and **Movie S6**). However, it
188 resulted in the misalignment of RN2+ neurons, which displayed scarce and long dendrites, and
189 in the formation of heterogeneous axon bundles (**Figure 6D)**.

190 In conclusion, the condensation of the VNC and the coordination of the peristaltic movements
191 leading to larval hatching are both dependent on precise levels of JNK activity in pioneer
192 neurons at the beginning of CNS morphogenesis. Early, JNK modulates the establishment of
193 the pioneer landscape and alterations in its activity induce aberrations in the axonal scaffold,
194 in cell bodies positioning, and in the coordination of muscles activity. Late, JNK impinges
195 upon the final refinement of the allocation of neurons and axonal tracts, but it is unrelated to
196 motor control (**Figure 6H**).

197

198 **DISCUSSION**

199 **JNK signaling coordinates motor activities**

200 In the *Drosophila* embryo, muscles become active very early and isolated twitches and
201 unilateral waves of contraction occur prior to the generation of propagated action potentials [29].
202 This stochasticity eventually evolves towards organized coordinated muscle contractions that
203 will promote the hatching of newborn larvae. We asked if pioneer neurons and the architectural
204 organization of the VNC have any functional significance in this context. Our data strongly
205 advocate for a close relationship between the acquisition of VNC architectural robustness and
206 the rhythmic coordination of motor functions. Mutant embryos of different *puc* alleles and
207 those overexpressing Hep^{CA} in pioneer neurons show severe structural defects (Karkali et al,
208 co-submitted) and also slower and uncoordinated muscle twitching; they never hatch.

209 The failure of motor coordination could be explained as an indirect result of firing defects [30],
210 associated to the aberrant dendritic arborizations of pioneer motoneurons observed when
211 altering the level of JNK activity. Dendrites carry the vast majority of synaptic inputs and their
212 morphology and properties are essential for propagation of postsynaptic potentials [31]. Indeed,
213 JNK signaling has been previously shown to promote dendrite pruning in *Drosophila* sensory
214 neurons [16]. Further, at the larval neuromuscular junction (NMJ), JNK signaling affects bouton
215 number and alters the amplitude of excitatory junction potentials (EJP) and spontaneous
216 responses. The sustained postembryonic JNK activation triggers synaptic growth, while the
217 strength of the synapses is reduced [8, 14]. Last, it has been suggested that JNKs might also be
218 involved in developmental neuroplasticity as JNKs are activated by environmental stimulation
219 and by electroconvulsive seizures in mice models [20].

220 A remarkable consequence of increasing JNK activity in pioneer motoneurons is the

221 hyperpolarization of their membranes (**Figure 6**) and it is well known that the membrane
222 potential can regulate cell differentiation as well as cortical tissue arrangement, shape and size.
223 Conceivably, in RN2 neurons, synaptic integration may be affected by changes in dendritic
224 arborization and morphology associated to high JNK activity. This in turn may affect the
225 frequency or capability of firing action potentials. Indeed, it is known that hyperpolarizing
226 conditions lead to a reduction of the number of connections in immature neurons *in vitro* [32].
227 Along these arguments, the hyperpolarization of RN2 cells after Hep^{CA} overexpression may in
228 part account for their anomalous dendritic arborization. Less probable would be a direct effect
229 in the implementation of motor coordination. If this were the case, the hyperpolarization of
230 RN2 cells should be linked to JNK early functions which, considering that action potentials
231 generate at late embryonic stages [29], is unlikely. Our results thus suggest that muscle
232 coordination failure will be primarily associated to the structural defects of the VNC after early
233 hyperactivation of the JNK pathway in pioneer neurons (**Figure 7**).

234

235 **JNK and the Cell Biology and Physiology of pioneer neurons**

236 It has been reported that the JNK cascade in the CNS regulates microtubule dynamics by
237 phosphorylating both, microtubule-associated proteins, including Tau [33], or the kinesin heavy
238 chain (Khc), which induces the kinesin motor to release from microtubules [11]. In the
239 *Drosophila* VNC, Tau together with microtubule-binding spectraplakins modulates
240 microtubule stability, which leads to alterations of JNK signaling activity, consequently
241 affecting kinesin-mediated axonal vesicle transport [13]. In our hands, however, interfering in
242 RN2 pioneer motoneurons JNK activity does not significantly affect synaptic vesicles transport
243 (**Figure S2**), although it inhibits mitochondrial motility (**Figure 3**), an effect previously
244 observed in third instar larvae, where the JNK pathway mediates the inhibition of
245 mitochondrial anterograde transport by oxidative stress [12]. These data suggest that the influence
246 of JNK signaling in conveying vesicles movements is probably cell and developmental stage
247 specific and, significantly, indicate that synaptic vesicles axonal transport in pioneer neurons
248 is irrelevant for embryos motor coordination. In addition, although it is known that JNK activity
249 perturbs neuronal migration during cortical development in mice [18, 34], we have not observed
250 any relevant drift of pioneer neurons when their level of JNK activity is altered.

251 While altering JNK signaling affects the cell biology (axonal transport) and physiology
252 (hyperpolarization) of pioneer neurons, we do not know if it does so through its well-

253 established role regulating gene expression, phosphorylating substrates such as Jun or histone
254 modifiers, or, alternatively, acts via the phosphorylation of cytoplasmic targets. The fact that,
255 in different models, the JNK pathway mediates microtubule destabilization leading to a
256 transport roadblock by phosphorylating cytoplasmic substrates, including microtubule-
257 associate proteins [33, 35], strongly supports this last possibility.

258

259 **Wiring Optimization**

260 It is well-established that spontaneous activities that persistently stimulate postsynaptic cells
261 result in long-term synapse potentiation [36]. These activities propagate efficiently between
262 nearby cells, ensuring connections are strengthened, whereas those from distant ones are lost
263 [37]. Bringing neurons in proximity improves functional interconnectedness and improves wiring
264 optimization [2]. We suggest that these classic principles are followed during the coordination of
265 motor activities in the *Drosophila* embryo. Several arguments support this premise. First, both
266 VNC condensation and motor coordination require a precise level of JNK activity at early
267 developmental stages, enabling activity of pioneer neurons (**Figure 6**). Second, either
268 activation or ablation of the EL interneurons disrupt bilateral muscle contractions in the larvae
269 [38]. Remarkably, these ELs make presynaptic contacts with the RP2 motoneurons, which we
270 found critical for both, the architectural organization of the VNC (Karkali et al, co-submitted)
271 and for motor coordination (**Figures 2** and **6**). Third, ELs, and the dorsal projecting
272 motoneurons they innervate, are nearly all *puc*-expressing neurons (Karkali et al, co-
273 submitted).

274 We foresee that the principles of wiring optimization may also apply at a postembryonic level.
275 As larvae develop, their body wall area grows by two orders of magnitude [39]. To accommodate
276 such a change, the mechanosensory neurons must extend their dendrites and increase their
277 receptive field [40], while motoneurons add more synapses to adapt to larger muscles [39, 41]. During
278 scaling, synaptic contacts between nearby neurons are sustained [42]. In this scenario, a post-
279 synaptic neuron can only connect with nearby specific pre-synaptic sites. The propensity to
280 form stable local functional synapses appears to operate across development.

281 Here we uncovered an intimate causal link between the temporal control of the activation of
282 the JNK pathway in pioneer neurons, the structural organization of axonal networks, VNC
283 condensation, and embryonic motor coordination (**Figure 7**). Correlative geometrical and
284 mechanical studies and further cell type-specific genetic interference analyses will be necessary

285 to dissect the precise mechanisms underlying this process. Yet, wiring optimization across
286 different circuits, by enhancing partners' proximity and topographical robustness, appears to
287 be an essential character associated with the morphogenesis of the nervous system.

288

289

290 **METHODS**

291

292 **Drosophila strains**

293 The following stocks were used:

294 *w1118*; *puc*^{E69}*LacZ/TM3, twi-GFP* [43]

295 *w1118*; *P{w[+mC]=UAS-Hep.Act}2* (BDSC #9306)

296 *w1118*; *P{w[+mC]=eve-Gal4.RN2}T, P{w[+mC]=UAS-mCD8::GFP.L}; P{w[+mC]=eve-*
297 *Gal4.RN2}G, P{w[+mC]=UAS-mCD8::GFP.L}* (Dr. Irene Miguel-Aliaga)

298 *w1118 P{w[+mW.hs]=GawB}MzVUM; P{y[+t7.7]w[+mC] = 10xUAS-IVS-mCD8::GFP}*
299 *attP40* (Dr. Irene Miguel-Aliaga)

300 *w1118*; *G203:UAS-TNT; ZCL2144* [7] (Dr. Matthias Landgraf)

301 *w1118*; *; ZCL2144* [7] (Dr. Matthias Landgraf)

302 *w1118; P{UAS-syt.eGFP}2* (BDSC #6925)

303 *w[1118]; P{w[+mC]=UAS-mitoGFP.AP}2 / CyO* (BDSC #8442)

304

305 In all cases, unless otherwise stated, embryos of the *w1118* strain served as controls.

306

307 **Genetics**

308 All crosses were performed at room temperature and after 48 hours were shifted to different
309 temperatures as the individual experiments required.

310 For temperature shifts, 2 hours embryo collections were done at room temperature in agar
311 plates and aged for a further 2 hours. Then, they were transferred, either to a 29ºC incubator

312 for 4 hours and then to an 18ºC incubator for 12 additional hours [Hep^{CA} (10-13)] or to an 18ºC
313 incubator for 12 hours and then to a 29ºC incubator for 4 hours [Hep^{CA} (15-16)]. These timing
314 regimes were calculated to enhance Hep^{CA} expression during the early pioneering stages or
315 during the final cell allocation and axonal refinement stages of VNC development. After the
316 temperature shifts the embryos were processed for immunocytochemistry or for live imaging.

317

318 **Immunohistochemistry**

319 Immunostaining of flat-prepped stage 16 *Drosophila* embryos was performed using the
320 primary antibodies: mouse anti-Fas 2 (1:100, clone 1D4, DHSB), and rabbit anti-GFP tag
321 polyclonal (1:600, Thermo Fisher Scientific, #A11122).

322 The secondary antibodies used for detection were: Goat anti-Rabbit IgG (H+L), Alexa Fluor
323 488 conjugate (A-11008) and Goat anti-Mouse IgG (H+L) Alexa Fluor 555 conjugate (A-
324 21422). All secondary antibodies were used in a dilution of 1:600 and were from Invitrogen.

325

326 **Sample preparations for immunodetection and image acquisition**

327 *Drosophila* embryo dissections for generating flat preparations were performed according to
328 [25]. Briefly, flies maintained in apple juice-agar plates at 25ºC were synchronized by repetitive
329 changes of the juice-agar plate, with a time interval of 2 hours. All embryos laid within this
330 time window were aged at different temperatures following experimental requirements until
331 reaching mid-stage 16 (3-part gut stage). At this point embryos were dechorionated with bleach
332 for 1 min, poured into a mesh and rinsed extensively with water. For dissection, embryos were
333 transferred with forceps on the surface of a small piece of double-sided tape, adhered on one
334 of the sides of a poly-L-Lysine coated coverslip. After orienting the embryos dorsal side up
335 and posterior end towards the center of the coverslip, the coverslip was flooded with saline
336 (0.075 M Phosphate Buffer, pH 7.2). Using a pulled glass needle the embryos were manually
337 de-vitelinized and dragged to the center of the coverslip, where they were attached to the coated
338 glass with their ventral side down. An incision on the dorsal side of the embryo was performed
339 using the glass needle from the anterior to the posterior end of the embryo. The gut was
340 removed by mouth suction and a blowing stream of saline was used to flatten their lateral
341 epidermis. Tissue fixation was done with 3.7 % formaldehyde in saline for 10 minutes at room
342 temperature. After this point standard immunostaining procedures were followed.

343 Image acquisition was performed on a Zeiss LSM 700 inverted confocal microscope, using a
344 40X oil objective lens (NA 1.3). Z-stacks, spanning the whole VNC thickness, were acquired
345 sectioning with a step size of 1 μm. Image processing was performed with Fiji [44].

346

347 **Live imaging**

348 Dechorionated stage 14 embryos were glued ventral side down on a MatTek glass bottom dish
349 and they were covered with S100 Halocarbon Oil (Merck) to avoid desiccation. Image
350 acquisition was performed on a Zeiss LSM 700 inverted confocal microscope, using a 25X oil
351 immersion lens (N.A 0.8, Imm Korr DIC M27). Z-stacks spanning the whole VNC thickness,
352 with a 2 μm step size, were acquired every 6 minutes for a total of 8 hours. Processing of time-
353 lapse data was done with Fiji [44].

354

355 **Image analysis**

356 Image analysis and quantification of fluorescence intensity were performed using Fiji [44]. In
357 immunostainings where quantification of the fluorescent intensity was required, extra care was
358 taken so that the same antibody batch was used for staining embryos of different genotypes,
359 while identical confocal acquisition settings were applied.

360

361 **Statistical analysis**

362 All statistical analyses were performed using GraphPad Software (GraphPad Software Inc., La
363 Jolla, CA, USA). In all cases one sample t test was performed and probability values $p<0.05$
364 were considered as significant.

365

366 **Muscle contraction analysis**

367 Stage 17 embryos carrying the G203, ZCL2144 or both GFP muscle markers were
368 dechorionated and mounted in halocarbon oil (3:1 mix of S700 and S27) following standard
369 procedures. Muscle contractions were monitored at the embryo's middle plane, using a 25X
370 oil immersion lens (N.A 0.8, Imm Korr DIC M27) in a Zeiss LSM780 confocal microscope.
371 For each acquisition 1000 frames were obtained with a scanning speed of 200 msec per frame

372 with a time interval between acquisition cycles of 15 minutes. Muscle activity was monitored
373 up to embryo's hatching or for a total of 12 hours at room temperature. For the experiments
374 where Hep^{CA} over-expression in RN2 and MzVum neurons was required, both control and
375 Hep^{CA} overexpressing embryos were filmed at 29ºC for equal time periods. For temperature-
376 shift analyses of animals expressing Hep^{CA} in RN2 neurons, embryos of equivalent pre-
377 hatching age were recorded at 200 msec per frame for 500 frames. Post-imaging, movies were
378 processed with Fiji [44] and Kymographs were generated using the Fiji plugin
379 KymoResliceWide.

380

381 **Axonal Trafficking**

382 To examine axonal trafficking, stage 17 embryos expressing UAS-Syt-GFP were
383 dechorionated and mounted laterally in halocarbon oil (3:1 mix of S700 and S27) for live
384 imaging. Synaptic vesicle transport was monitored in the medial part of the Inter-Segmental
385 Nerve (ISN) using a 40X oil immersion lens (N.A 1.3, Oil DIC M27) in a Zeiss LSM780
386 confocal microscope. A constant frame size of 512x100 pixels, with an XY zoom of 6 and a
387 recording line spacing of 2 were routinely employed. Single plane movies were acquired with
388 a scanning speed of 1.11 sec, with 1 sec interval for a total of 60 cycles. All movies were
389 processed with Fiji and Kymographs were generated using the Fiji plugin KymoResliceWide.

390 The Mean Velocity and the Lifetime parameters for each particle were calculated from the
391 Kymographs as follows. The particles trajectories were traced and saved as independent ROIs.
392 The XY coordinates for each ROI were then extracted using the getSelectionCoordinates
393 function in Fiji of the custom made "Macro coordinates.ijm" shown below:

```
394 run ("Fit Spline", "straighten");
395 getSelectionCoordinates (x, y);
396   x2=0; y2=0; distance=0;
397   for (i=0; i<x.length; i++) {
398       if (i>0) {
399           dx = x[i] - x[i-1];
400           dy = y[i] - y[i-1];
```

```
401            distance = sqrt(dx*dx+dy*dy);
402          }
403          print (i, x[i], y[i], distance);
404      }
```

405 These XY coordinates represent the particles displacement in both space (X values) and time
406 (Y values), thus permitting the calculation of Mean Velocity and Lifetime.

407

408 **Analysis of Axonal and dendrite morphology by Segmentation**

409 To describe the axonal and dendrite morphology of the RN2+ neurons, we analyzed images of
410 flat-prepped embryos immunostained against GFP and Fasciclin 2 using the Simple Neurite
411 Tracer Fiji plugin [45]. Image segmentation by this tool allows a semi-automated tracing of axons
412 and dendrites in 3D, providing measurements of total axonal and dendrite length, as well as of
413 dendrite number directly from skeletonized images.

414

415 **Embryo whole-cell patch-clamp recordings**

416 Dissections and recordings were performed as described [29] at room temperature (20-22°C).
417 Late stage 17 *Drosophila* embryos were dissected in external saline (in mM: 135 NaCl, 5 KCl,
418 4 MgCl2·6H2O, 2 CaCl2·2H2O, 5 N-Tris[hydroxymethyl]methyl-2-aminoethanesulfonic
419 acid, and 36 sucrose, pH 7.15). The CNS was exposed through a dorsal-longitudinal cut of the
420 dechorionated embryonic body wall musculature. Embryonic cuticle was secured to a Sylgard
421 (Dow-Corning, Midland, Michigan, USA)-coated cover slip using tissue glue (GLUture; WPI,
422 Hitchin, UK) and larval gut and fat body removed. The glia surrounding the CNS was partially
423 removed using protease (1% type XIV; Sigma, Dorset, UK) contained in a wide-bore (15 µm)
424 patch pipette. Whole cell recordings were carried out using borosilicate glass electrodes
425 (GC100TF-10; Harvard Apparatus, Edenbridge, UK), fire-polished to resistances of between
426 16-20 MΩ. Cell identity was confirmed through RN2-GAL4 driven expression of UAS-CD8-
427 GFP. Recordings were made using a MultiClamp 700B amplifier. Endogenous excitatory
428 synaptic cholinergic input to the aCC/RP2 motoneurons were recorded in voltage clamp and
429 current clamp sampled at 20 kHz and low pass filtered at 10 kHz, using pClamp 10.6

(Molecular Devices, Sunnyvale, CA). Only neurons with an input resistance of ≥ 1GΩ were accepted for analysis.

ACKNOWLEDGEMENTS

We are extremely grateful to all colleagues that have provided us materials, training and guidance throughout this work as well as for commenting on the manuscript. Amongst them we like to specially thank Christian Klambt, Claude Desplan, Matthias Landgraf, Chris Doe and Brian McCabe. We also thank our colleagues at the IBMB and the BSRC "Alexander Fleming" for their encouragement and support. The Martín-Blanco laboratory was supported by funds from Ministry of Innovation and Science (BFU2014-57019-P and BFU2017-82876-P) and Fundación Ramón Areces. RAB was supported by a BBSRC BB/L027690/1 grant and SWV by a BBSRC CASE studentship. Work on this project benefited from the Manchester Fly Facility with funds from University and the Wellcome Trust (087742/Z/08/Z).

FIGURES

Figure 1

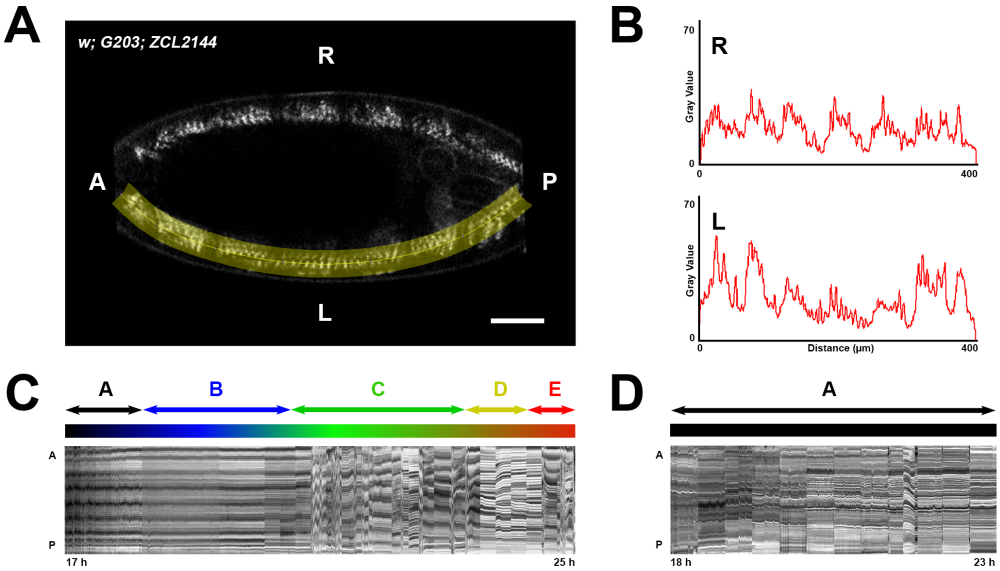

446

447

448

449 **Figure 1. Defective motor coordination results in incomplete peristalsis in *puc*^{E69} embryos**

450 **A)** Representative mid-plane image of a stage 17 embryo carrying two GFP protein traps
451 expressed at muscle Z-lines (*w; G203; ZCL2144*) (see **Movie S1**). A selected segmented-line
452 (highlighted in yellow) was employed to create kymographs spanning muscle units along the
453 A/P axis (see below) at both sides of the embryo, right (R) and left (L). The evolution overtime
454 of these kymographs was monitored live. Scale bar is 25 µm. **B)** Intensity Profile plots
455 generated along the segmented-line selection in **A**. Gray values as a function of distance
456 highlight the distribution of the segmental muscle units along the axis. Muscle contraction is
457 detected by the differences in the distance between consecutive peaks at sequential time points.
458 **C)** Kymograph displaying muscle profiles from 17 to 25 hours AEL for the left side of the
459 embryo in **A**. Anterior (A) and posterior (P). Motor coordination maturation occurs in 5 stages
460 of approximated stereotyped length (color coded): A, Intense unilateral twitching; B, general
461 inactivity with occasional uncoordinated contractions; C, initiation of backward and forward
462 peristalsis; D, pre-hatching inactivity period and E, complete peristalsis and specialized
463 hatching head movements. **D)** Kymograph displaying muscle profiles from 18 to 23 hours
464 AEL, when the embryo dies, for the left side of a *puc*^{E69} embryo (see **Movie S8**). Anterior (A)
465 and posterior (P). Motor coordination fails and embryos do not progress beyond the unilateral
466 contraction period (stage A).

Figure 2

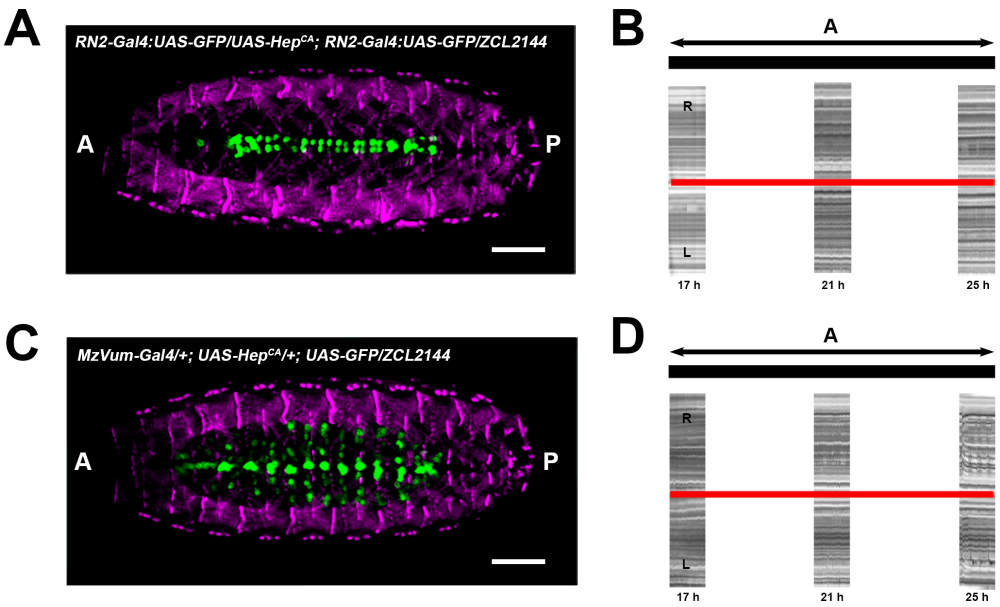

467

468

469

470 **Figure 2. JNK activity modulates embryo motor coordination**

471 **A** and **C** Ventral view of stage 17 embryos expressing GFP under the control of the RN2-Gal4
472 (**E**) and MzVum-Gal4 (**G**) lines co-expressing Hep^{CA} and carrying the muscle Z-lines specific
473 GFP protein trap ZCL2144. Muscles are pseudo-colored in magenta and neurons in green.
474 Scale bar is 25 µm. **B** and **D**) Kymographs (ZCL2144 marker) revealing occasional unilateral
475 contractions in embryos co-expressing Hep^{CA} in the RN2-Gal4 (**F**) and MzVum-Gal4 (**H**)
476 neurons. For each case, the kymographs correspond to three periods of 1 hour. These embryos
477 never manage to coordinate muscle movements. Both sides, right (R) and left (L) are sh

Figure 3

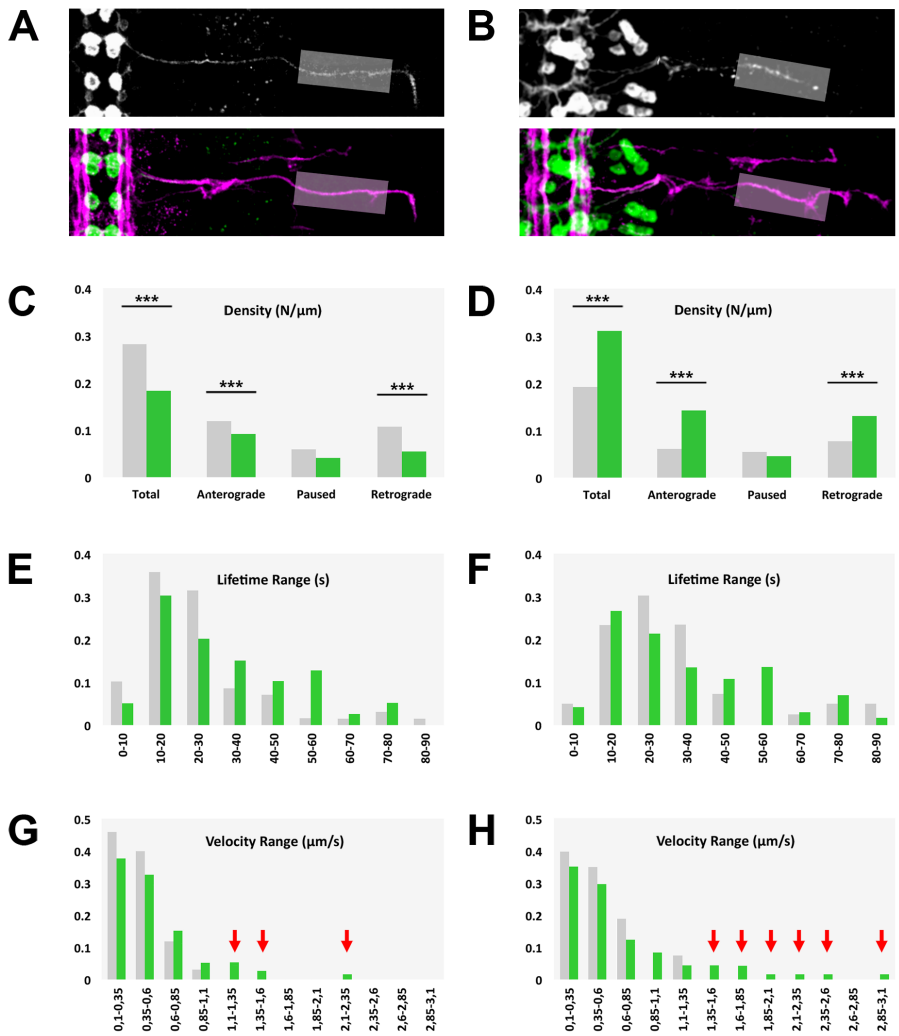
A
B
C
Density (N/µm)
***
Total
Anterograde
Paused
Retrograde
D
Density (N/µm)
E
Lifetime Range (s)
0-10
10-20
20-30
30-40
40-50
50-60
60-70
70-80
80-90
F
Lifetime Range (s)
G
Velocity Range (µm/s)
0,1-0,35
0,35-0,6
0,6-0,85
0,85-1,1
1,1-1,35
1,35-1,6
1,6-1,85
1,85-2,1
2,1-2,35
2,35-2,6
2,6-2,85
2,85-3,1
H
Velocity Range (µm/s)

481 **Figure 3. JNK activity affects mitochondrial axonal transport**

482 **A** and **B**) Flat-prepped, stage 16 embryos expressing Mito-GFP under the control of the RN2-
483 Gal4 (**A**) and MzVum-Gal4 (**B**) lines immunostained for GFP (gray scale - top panels and green
484 - bottom panels) and Fas 2 (magenta - bottom panel). The grey rectangle marks the medial part
485 of the ISN, where mitochondrial axonal transport was monitored (see **Movie S3**). Scale bar is
486 25 µm. **C** and **D**) Histograms showing mitochondrial density and directional motility in control
487 (grey) versus Hep^{CA} expressing (green) aCC/ RP2 (**C**) and VUM motoneurons (**D**). Statistically
488 significant differences ($p<0.001$) were observed between control and JNK overactive neurons.
489 **E** and **F**) Lifetime range distribution of motile mitochondria in aCC/RP2 (grey) and Hep^{CA}
490 expressing (green) embryos. **G** and **H**) Mean velocity range distribution comparison of motile
491 mitochondria in aCC/RP2 (**G**) and VUM (**H**) motoneurons between control (grey) and JNK
492 gain-of function (green) conditions. For both sets of motoneurons the distribution was shifted
493 to higher velocity classes in JNK hyperactive neurons.

Figure 4

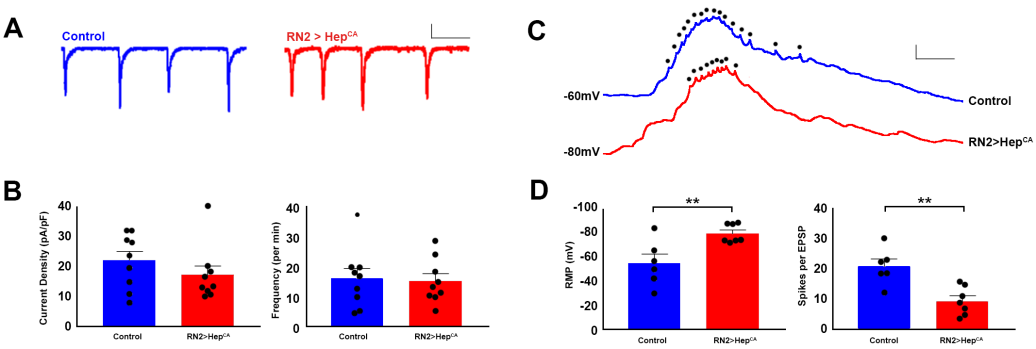

494

495

496

497 **Figure 4. JNK activity modulates neuronal firing**

498 **A)** Representative traces of endogenously produced cholinergic SRCs from aCC/RP2
499 motoneurons in late stage 17 embryos in control (*RN2-Gal4 / CyO*) and experimental lines
500 (*RN2-Gal4 > UAS-Hep*^{CA}). Scale Bar: 20 pA / 2s. **B)** No significant difference in SRC
501 amplitude (21.7 ± 3.0 vs. 17.0 ± 3.1 pA / pF, control vs. *RN2-Gal4 > UAS-Hep*^{CA} respectively,
502 P = 0.28) or frequency (16.3 ± 3.3 vs. 15.4 ± 2.4 per min, P = 0.83) was observed. **C)**
503 Representative traces of endogenously produced cholinergic EPSPs from aCC/RP2
504 motoneurons in late stage 17 embryos in control (*RN2-Gal4 / CyO*) and experimental lines
505 (*RN2-Gal4 > UAS-Hep*^{CA}). Action potentials are indicated by dots. The amplitude of the action
506 potentials is shunted because of the underlying depolarization. Scale Bar: 10 mV / 100ms. **D)**
507 Motoneuron resting membrane potential (RMP) is significantly hyperpolarized in *RN2-Gal4 >*
508 *UAS-Hep*^{CA} (-57.0 ± 7.6 vs. -81.5 ± 2.9 mV, control vs. *RN2-Gal4 > UAS-Hep*^{CA} respectively,
509 P = 0.009). Consequently, the average number of action potentials fired per EPSP was also
510 significantly reduced (20.6 ± 2.4 vs. 9.3 ± 1.7 spikes per EPSP, P = 0.003). All data points are
511 shown on graphs, bars represent mean ± sem.

Figure 5

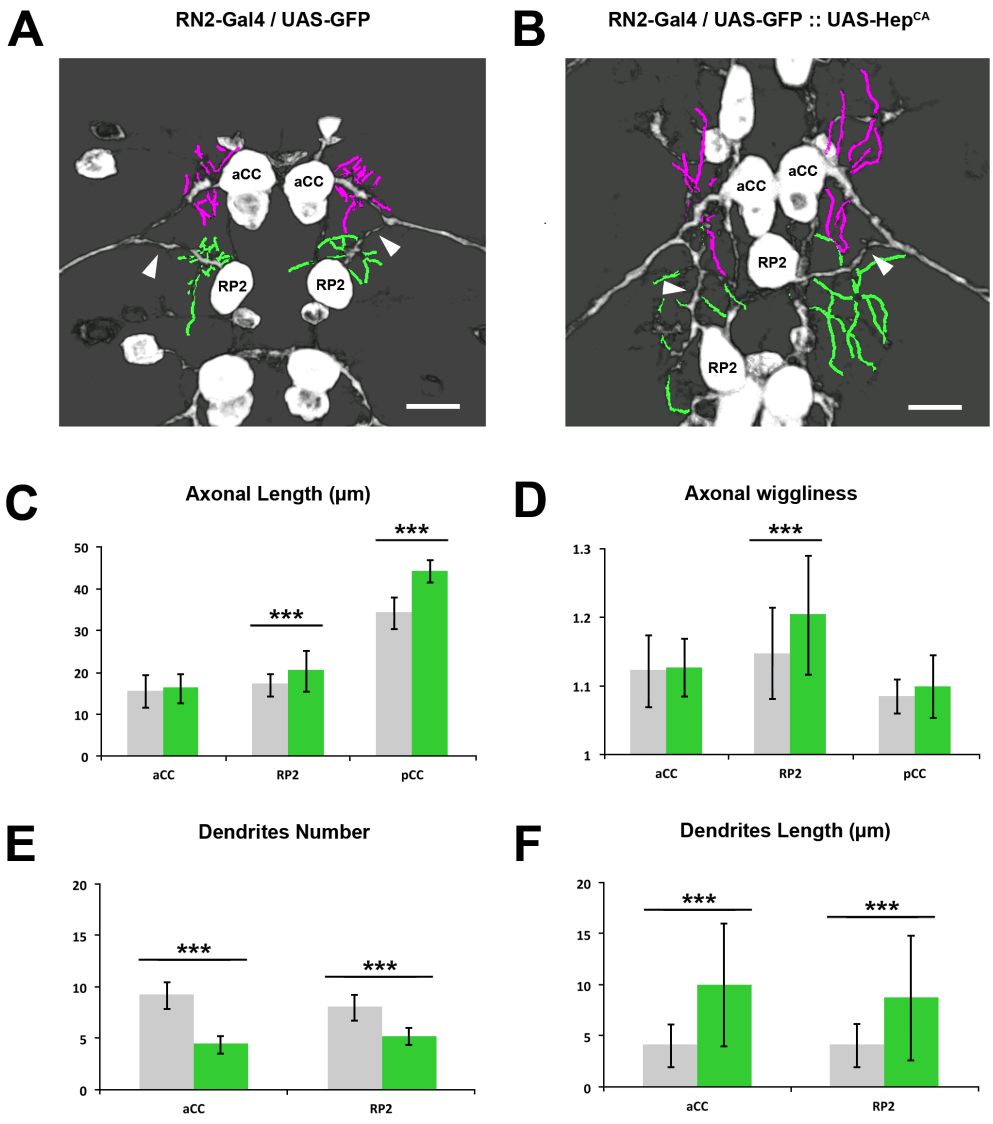

512

513

514 **Figure 5. The axonal and dendritic landscape of pioneer neurons is altered upon JNK**
515 **hyperactivation**

516 **A** and **B**) Flat-prepped, stage 16 embryos expressing mCD8-GFP (**A**) and mCD8-GFP and
517 Hep^{CA} (**B**) under the control of the RN2-Gal4 line immunostained for GFP. Traces of the aCC
518 (magenta) and RP2 (green) proximal dendrites are over-imposed. Yellow arrowheads point to
519 differences in RP2 axon morphology. Anterior is up. Scale bar is 10 µm. **C**) Histograms
520 showing the average axonal length of the aCC, RP2 and pCC neurons. Statistically significant
521 differences ($p<0.001$) in the axonal length of the RP2 and pCC neurons were detected between
522 control and Hep^{CA} expressing neurons (n= 4 embryos). Control embryos are represented in
523 grey and Hep^{CA} expressing embryos in green. **D**) Histograms showing the average axonal
524 wiggliness of the aCC, RP2 and pCC neurons. RP2 axonal wiggliness was found significantly
525 increased after Hep^{CA} expression ($p<0.001$, n= 4 embryos). **E** and **F**) Graphs representing the
526 average Dendrite Number (**E**) and average Dendrite Length (**F**) of the aCC and RP2 neurons.
527 In all cases significant differences were scored in the comparison of control and Hep^{CA}
528 expressing embryos ($p<0.001$, n= 4 embryos).

Figure 6

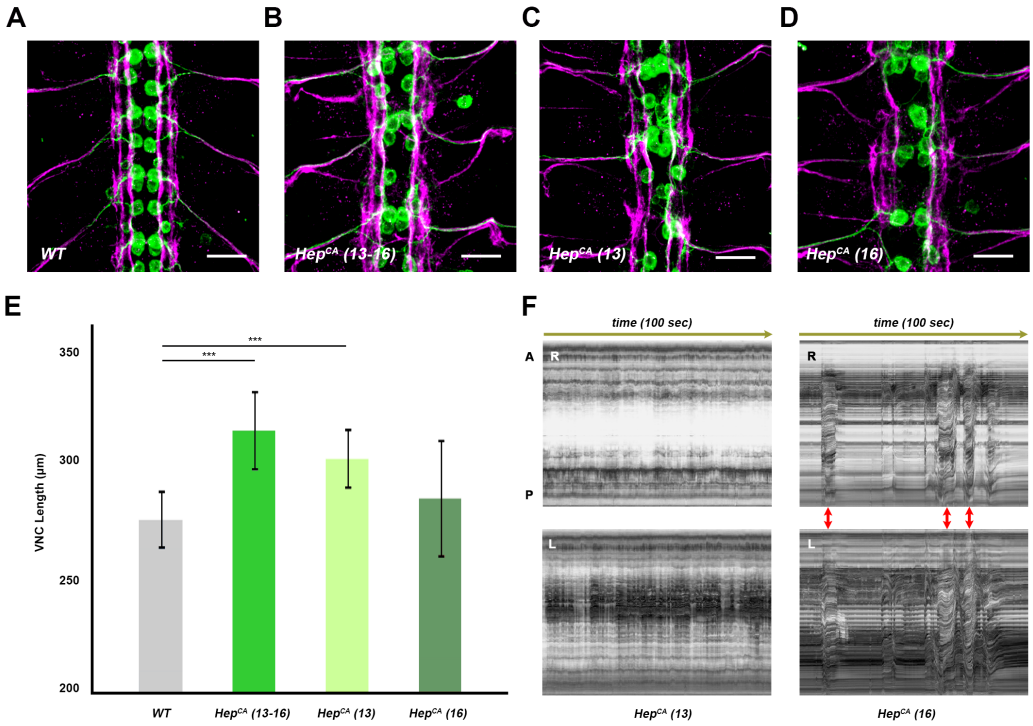

529

530

531

532 **Figure 6. JNK activity modulates VNC condensation and embryo motor coordination**

533 **A-D)** Fas 2 (magenta) and GFP (green) immunoreactivity of RN2-Gal4 embryos at late stage
534 16 subjected to different temperature shift conditions and expressing, from left to right: (**A**)
535 GFP alone (WT) (maintained at 29ºC continuously from stage 10 to 16); or GFP in combination
536 with a *Hep*^{CA} transgene; Hep^{CA} (10-16) (maintained at 29ºC continuously from stage 10 to 16)
537 (**B**); Hep^{CA} (10-13) (kept at 29ºC between stages 10 and 13) (**C**) and Hep^{CA} (15-16) (kept at
538 29ºC during stages 15 and 16) (**D**). Maximum projection of ventral views across three VNC
539 abdominal segments. Scale Bar is 10 µm. Overexpressing *Hep*^{CA} at early stages affects pioneer
540 functions and provoke the collapse of neurons cell bodies into the midline. At late stages,
541 dendrite arborizations, axons fasciculation and cell bodies alignment are disturbed. **E)**
542 Quantification of the VNC length in µm (average and standard deviation) for each condition
543 above. Statistically significant differences in length ($p < 0.0001$) were detected between WT
544 and (Hep^{CA} 10-16) and (Hep^{CA} 10-13) embryos. **F)** Kymographs (bright field) displaying
545 muscle profiles at 25 hours AEL (100 sec) for the left (L) and right (R) sides of embryos
546 expressing Hep^{CA} in RN2+ cells at early (10-13) or late (15-16) developmental stages. Anterior
547 (A) and posterior (P). Embryos overexpressing *Hep*^{CA} at early stages in RN2+ neurons never
548 managed to coordinate muscle movements but those overexpressing *Hep*^{CA} late, developed
549 bilaterally symmetrical peristalsis (red arrows) and hatched in all occasions (**Movie S6**).

Figure 7

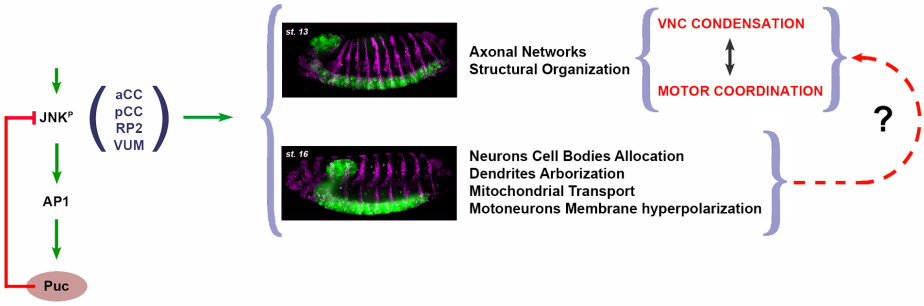

550

551

552 **Figure 7. The early activity of the JNK pioneer neurons affects the structural**
553 **organization of axonal networks and motor activity coordination**

554 Precise JNK activity levels in early-specified neurons (at least aCC, pCC, RP2 and VUMs) are
555 regulated by a negative feedback loop mediated by Puc. Excessive JNK activity in *puc* mutants
556 or upon overexpressing HepCA in aCC, pCC, RP2 and/or VUMs leads to autonomous defects
557 in axonal paths and dendrites numbers and shape, mitochondrial axonal transport and
558 hyperpolarization of motoneurons membranes. Further, the architectural robustness of the
559 VNC is affected, its condensation prevented and the coordination of embryonic motor activities
560 and peristaltic movements inhibited. The incomplete condensation of the VNC may result in a
561 failure in wiring optimization, partly responsible of motor uncoordination .

562 **REFERENCES**

563 1. Huntenburg JM. A core organizing axis of the human cerebral cortex.). Freie
564 Universität Berlin (2018).

565 2. Cajal SRy. *Textura del Sistema Nervioso del Hombre y de los Vertebrados* Nicolas
566 Moya (1899).

567 3. Tessier-Lavigne M, Goodman CS. The molecular biology of axon guidance. *Science*
568 **274**, 1123-1133 (1996).

569 4. Chklovskii DB, Koulakov AA. Maps in the brain: what can we learn from them?
570 *Annual review of neuroscience* **27**, 369-392 (2004).

571 5. Huntenburg JM, Bazin PL, Margulies DS. Large-Scale Gradients in Human Cortical
572 Organization. *Trends Cogn Sci* **22**, 21-31 (2018).

573 6. Karkali K*, et al.* Condensation of the Drosophila nerve cord is oscillatory and depends
574 on coordinated mechanical interactions. *Dev Cell* **57**, 867-882 e865 (2022).

575 7. Crisp S, Evers JF, Fiala A, Bate M. The development of motor coordination in
576 Drosophila embryos. *Development* **135**, 3707-3717 (2008).

577 8. Wang MC, Bohmann D, Jasper H. JNK signaling confers tolerance to oxidative stress
578 and extends lifespan in Drosophila. *Dev Cell* **5**, 811-816 (2003).

579 9. Kenney AM, Kocsis JD. Peripheral Axotomy Induces Long-Term c-Jun Amino-
580 Terminal Kinase-1 Activation and Activator Protein-1 Binding Activity by c-Jun and
581 junD in Adult Rat Dorsal Root Ganglia "In Vivo". *The Journal of Neuroscience* **18**,
582 1318-1328 (1998).

583 10. Srahna M, Leyssen M, Choi CM, Fradkin LG, Noordermeer JN, Hassan BA. A
584 signaling network for patterning of neuronal connectivity in the Drosophila brain. *PLoS*
585 *Biol* **4**, e348 (2006).

586 11. Morfini G, Pigino G, Szebenyi G, You Y, Pollema S, Brady ST. JNK mediates
587 pathogenic effects of polyglutamine-expanded androgen receptor on fast axonal
588 transport. *Nat Neurosci* **9**, 907-916 (2006).

589 12. Liao PC, Tandarich LC, Hollenbeck PJ. ROS regulation of axonal mitochondrial
590 transport is mediated by Ca2+ and JNK in Drosophila. *PLoS One* **12**, e0178105 (2017).

591 13. Voelzmann A*, et al.* Tau and spectraplakins promote synapse formation and
592 maintenance through Jun kinase and neuronal trafficking. *Elife* **5**, e14694 (2016).

593 14. Etter PD, *et al.* Synaptic and genomic responses to JNK and AP-1 signaling in
594 Drosophila neurons. *BMC Neurosci* **6**, 39 (2005).

595 15. Sanyal S, Sandstrom DJ, Hoeffer CA, Ramaswami M. AP-1 functions upstream of
596 CREB to control synaptic plasticity in Drosophila. *Nature* **416**, 870-874 (2002).

597 16. Zhu S, Chen R, Soba P, Jan YN. JNK signaling coordinates with ecdysone signaling to
598 promote pruning of Drosophila sensory neuron dendrites. *Development* **146**,
599 dev163592 (2019).

600 17. Xu D, Zhang F, Wang Y, Sun Y, Xu Z. Microcephaly-associated protein WDR62
601 regulates neurogenesis through JNK1 in the developing neocortex. *Cell Rep* **6**, 104-116
602 (2014).

603 18. Zhang F, *et al.* A Novel c-Jun N-terminal Kinase (JNK) Signaling Complex Involved
604 in Neuronal Migration during Brain Development. *J Biol Chem* **291**, 11466-11475
605 (2016).

606 19. Kuan CY, Yang DD, Samanta Roy DR, Davis RJ, Rakic P, Flavell RA. The Jnk1 and
607 Jnk2 protein kinases are required for regional specific apoptosis during early brain
608 development. *Neuron* **22**, 667-676 (1999).

609 20. Mielke K, Herdegen T. JNK and p38 stresskinases--degenerative effectors of signal-
610 transduction-cascades in the nervous system. *Prog Neurobiol* **61**, 45-60 (2000).

611 21. Crisp SJ, Evers JF, Bate M. Endogenous patterns of activity are required for the
612 maturation of a motor network. *J Neurosci* **31**, 10445-10450 (2011).

613 22. Suster ML, Bate M. Embryonic assembly of a central pattern generator without sensory
614 input. *Nature* **416**, 174-178 (2002).

615 23. Pereanu W, Spindler S, Im E, Buu N, Hartenstein V. The emergence of patterned
616 movement during late embryogenesis of Drosophila. *Dev Neurobiol* **67**, 1669-1685
617 (2007).

618 24. Baines RA, Robinson SG, Fujioka M, Jaynes JB, Bate M. Postsynaptic expression of
619 tetanus toxin light chain blocks synaptogenesis in Drosophila. *Curr Biol* **9**, 1267-1270
620 (1999).

621 25. Landgraf M, Bossing T, Technau GM, Bate M. The origin, location, and projections of
622 the embryonic abdominal motorneurons of Drosophila. *J Neurosci* **17**, 9642-9655
623 (1997).

624 26. Furrer MP, Vasenkova I, Kamiyama D, Rosado Y, Chiba A. Slit and Robo control the
625 development of dendrites in Drosophila CNS. *Development* **134**, 3795-3804 (2007).
626 27. Jacobs JR, Goodman CS. Embryonic development of axon pathways in the Drosophila
627 CNS. II. Behavior of pioneer growth cones. *J Neurosci* **9**, 2412-2422 (1989).
628 28. Sink H, Whitington PM. Pathfinding in the central nervous system and periphery by
629 identified embryonic Drosophila motor axons. *Development* **112**, 307-316 (1991).
630 29. Baines RA, Bate M. Electrophysiological development of central neurons in the
631 Drosophila embryo. *J Neurosci* **18**, 4673-4683 (1998).
632 30. Katz LC, Shatz CJ. Synaptic activity and the construction of cortical circuits. *Science*
633 **274**, 1133-1138 (1996).
634 31. Spruston N, Stuart G, Häusser M. Principles of dendritic integration. In: *Dendrites.* (eds
635 Spruston N, Stuart G, Häusser M). Oxford University Press (2016).
636 32. Ozkucur N*, et al.* Membrane potential depolarization causes alterations in neuron
637 arrangement and connectivity in cocultures. *Brain Behav* **5**, 24-38 (2015).
638 33. Bjorkblom B*, et al.* Constitutively active cytoplasmic c-Jun N-terminal kinase 1 is a
639 dominant regulator of dendritic architecture: role of microtubule-associated protein 2
640 as an effector. *J Neurosci* **25**, 6350-6361 (2005).
641 34. Yu J, Zhang F, Wang S, Zhang Y, Fan M, Xu Z. TAK1 is activated by TGF-β signaling
642 and controls axonal growth during brain development. *J Mol Cell Biol* **6**, 349-351
643 (2014).
644 35. Shin JE*, et al.* SCG10 is a JNK target in the axonal degeneration pathway. *Proc Natl*
645 *Acad Sci U S A* **109**, E3696-3705 (2012).
646 36. Hebb D. The Organization of Behavior: A Neuropsychological Theory. John Wiley
647 And Sons Inc; New York; Chapman And Hall Limited; London (1949).
648 37. Eglen SJ, Demas J, Wong RO. Mapping by waves. Patterned spontaneous activity
649 regulates retinotopic map refinement. *Neuron* **40**, 1053-1055 (2003).
650 38. Heckscher ES*, et al.* Even-Skipped(+) Interneurons Are Core Components of a
651 Sensorimotor Circuit that Maintains Left-Right Symmetric Muscle Contraction
652 Amplitude. *Neuron* **88**, 314-329 (2015).
653 39. Keshishian H, Chiba A. Neuromuscular development in Drosophila: insights from
654 single neurons and single genes. *Trends Neurosci* **16**, 278-283 (1993).

655 40. Grueber WB, Jan LY, Jan YN. Tiling of the Drosophila epidermis by multidendritic
656 sensory neurons. *Development* **129**, 2867-2878 (2002).

657 41. Rasse TM*, et al.* Glutamate receptor dynamics organizing synapse formation in vivo.
658 *Nat Neurosci* **8**, 898-905 (2005).

659 42. Gerhard S, Andrade I, Fetter RD, Cardona A, Schneider-Mizell CM. Conserved neural
660 circuit structure across Drosophila larval development revealed by comparative
661 connectomics. *Elife* **6**, e29089 (2017).

662 43. Martin-Blanco E*, et al.* puckered encodes a phosphatase that mediates a feedback loop
663 regulating JNK activity during dorsal closure in Drosophila. *Genes & development* **12**,
664 557-570 (1998).

665 44. Schindelin J*, et al.* Fiji: an open-source platform for biological-image analysis. *Nat*
666 *Methods* **9**, 676-682 (2012).

667 45. Longair MH, Baker DA, Armstrong JD. Simple Neurite Tracer: open source software
668 for reconstruction, visualization and analysis of neuronal processes. *Bioinformatics* **27**,
669 2453-2454 (2011).

670

671

SUPPLEMENTARY FIGURES

Figure S1

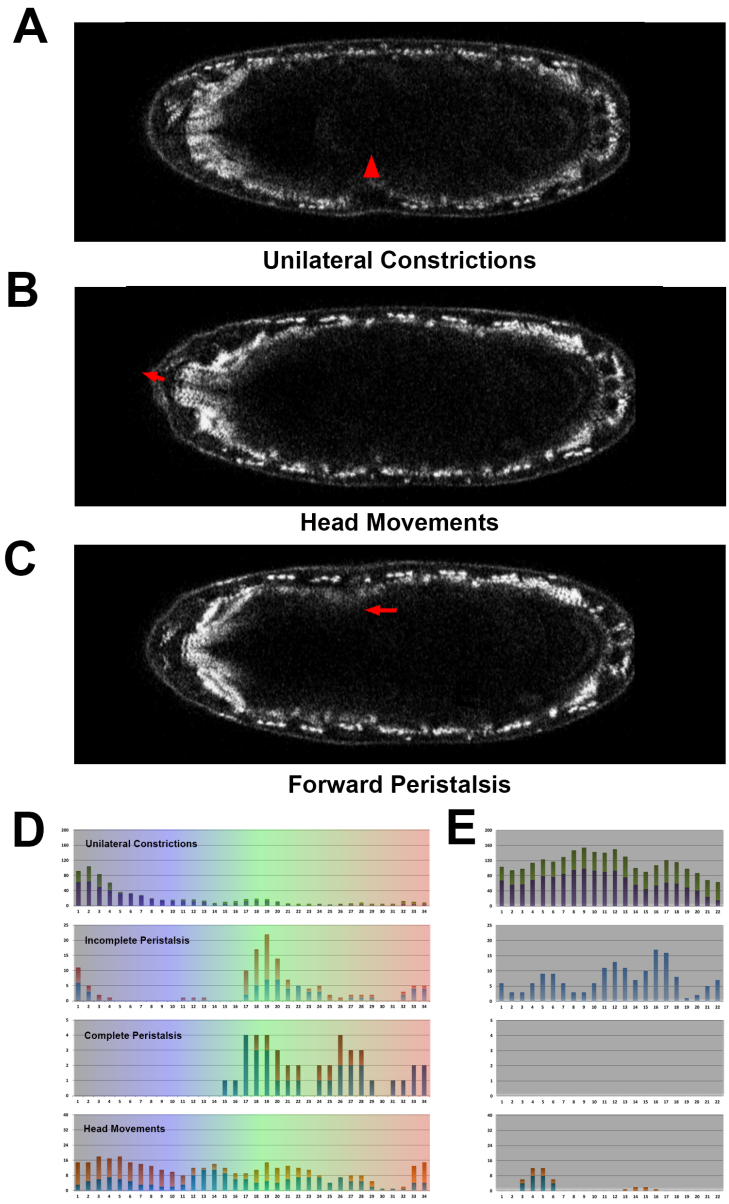

675 **Figure S1. Types of embryonic muscle movements**

676 Snapshots from **Movie S1** displaying mid-plane images of a stage 17 embryo carrying two GFP
677 protein traps expressed at muscle Z-lines (*w; G203, ZCL2144*). Three main types of movement
678 were observed during the muscle coordination process. Red arrows point to the contracting
679 muscle units. Anterior is to the left. Scale bar is 50 µm. **A)** Unilateral muscle contractions.
680 They can occur at any embryo side and in different segments. **B)** Head turning and mouth hook
681 pinching. **C)** Peristalsis. They can be incomplete or complete and develop forward (in the
682 image) or backward displacements. **D)** Histograms showing the progression of the muscle
683 coordination process in wild type embryos. Over-imposed colors follow the 5 stages of motor
684 coordination maturation described in **C**. Muscle movements were distributed in four classes:
685 Unilateral contractions [sum of the contractions occurring at the right (green) and the left
686 (purple) side of the embryo]; Incomplete peristalsis [sum of the incomplete forward (blue) and
687 incomplete backward (red) peristaltic attempts]; Complete peristalsis [sum of the full forward
688 (blue) and backward (red) peristalsis]; and Head movements [sum of head turning (red) and
689 mouth hook pinching events (blue)]. **E)** Histograms equivalent to **D** showing the unsuccessful
690 muscle coordination of puc^{E69} embryos.

Figure S2

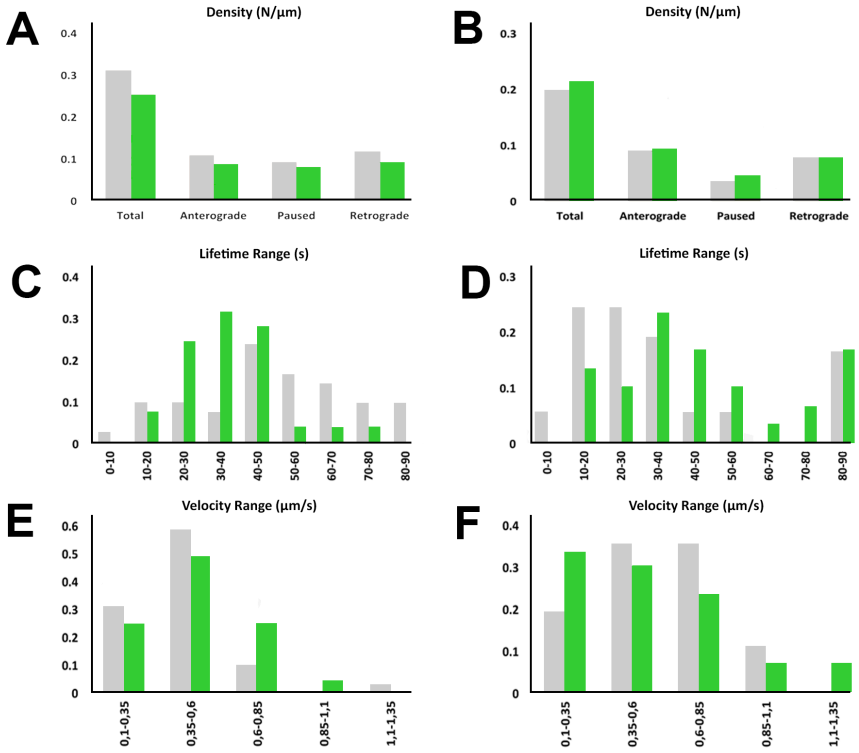

691

692

693 **Figure S2. Synaptotagmin transport is unaffected by JNK hyper-activation in aCC/RP2**
694 **and VUM motoneurons**

695 A and B) Histograms showing synaptotagmin vesicles density and directional motility in
696 control (grey) versus Hep^{CA} expressing (green) aCC/ RP2 (A) and VUM motoneurons (B). No
697 statistically significant differences were observed between control and JNK over-active
698 neurons. C and D) Lifetime range distribution of motile synaptotagmin vesicles in aCC/RP2
699 (C) and VUM (D) motoneurons. No differences were observed in lifetime between control
700 (grey) and Hep^{CA} expressing (green) embryos. E and F) Mean velocity range distribution
701 comparison of motile synaptotagmin vesicles in aCC/RP2 (E) and VUM (F) motoneurons
702 between control (grey) and JNK gain-of function (green) conditions. For both sets of
703 motoneurons the distribution was unaltered.

704

705

706 **SUPPLEMENTARY MOVIES LEGENDS**

707

708 **Movie S1. Embryonic motor patterns**

709 Representative mid-plane movies of a stage 17 embryo carrying two GFP protein traps
710 expressed at muscle Z-lines (*w; G203; ZCL2144*). **A)** Forward peristalsis. **B)** Backward
711 Peristalsis. **C)** Left twitch. **D)** Right twitch. **E)** Head tumble. **F)** Mandible pinch. Scale bar is
712 50 µm. Anterior is to the left.

713

714 **Movie S2. Time course of motor maturation**

715 Representative mid-plane movies (250 time points per stage) of an embryo carrying two GFP
716 protein traps expressed at muscle Z-lines (*w; G203; ZCL2144*). From top to bottom stages **A**
717 (Unilateral twitches and incomplete peristalsis), **B** (Resting period), **C** (Complete peristalsis),
718 **D** (Late resting period) and **E** (Hatching movements). Color coded as in **Figure 6**. Scale bar is
719 50 µm. Anterior is to the left.

720

721 **Movie S3. Motor activity of puc^{E69} embryos**

722 Representative mid-plane movie (1000 time points) of a late stage 17 *puc*^{E69} embryo carrying
723 two GFP protein traps expressed at muscle Z-lines (*w; G203; ZCL2144*). Scale bar is 50 µm.
724 Anterior is to the left.

725

726 **Movie S4. Synaptic vesicles axonal transport in RN2 neurons**

727 Stage 16 embryos expressing Synaptotagmin-GFP under the control of the RN2-Gal4 in the
728 absence **(A)** or presence **(B)** of Hep^{CA}. Left panels present representative single plane movies
729 (Fire Luts) with 1 sec interval for a total of 60 cycles. Right panels display in different colors
730 the traces of the different particles analyzed. Proximal is to the left. Scale bar is 25 µm.

731

732 **Movie S5. Axonal and dendritic landscape of pioneer neurons upon JNK hyper-activation**

733 Animated 3D reconstruction of the axonal and dendritic pattern of stage 16 embryos expressing
734 mCD8-GFP (**A**) and mCD8-GFP and Hep^{CA} (**B**) under the control of the RN2-Gal4 line. Traces
735 of the dendrites (purple) are over-imposed. Scale bar is 10 µm.

736

737 **Movie S6. Motor coordination responses to early and late JNK hyperactivation**

738 Representative mid-plane movies of stage 17 embryos expressing Hep^{CA} in RN2+ cells at early
739 (13 - top) or late (16 - bottom) developmental stages. Embryos over-expressing Hep^{CA} at early
740 stages never coordinate muscle movements but those overexpressing Hep^{CA} late, developed
741 multiple bilaterally symmetrical peristalsis and hatched. Scale bar is 50 µm